CHEMISTRY OF MATERIALS

Article

pubs.acs.org/cm

Highly Stable and Magnetically Recyclable Mesoporous Silica Spheres Embedded with FeCo/Graphitic Shell Nanocrystals for Supported Catalysts

Yan Li,[†] Yun Jin Kim,[†] A. Young Kim,[‡] Kyujoon Lee,[§] Myung Hwa Jung,[§] Nam Hwi Hur,[†] Kang Hyun Park,*[,‡] and Won Seok Seo*[,†]

[†]Department of Chemistry, Inorganic and Bio-Materials Center of BK21, Sogang University, Seoul, 121-742, Korea

[‡]Department of Chemistry and Chemistry Institute for Functional Materials, Pusan National University, Busan 609-735, Korea

[§]Department of Physics, Sogang University, Seoul, 121-742, Korea.

Supporting Information

ABSTRACT: We have synthesized highly stable and magnetically recyclable mesoporous silica spheres embedded with FeCo-graphitic carbon shell nanocrystals (FeCo/GC@MSS) by a simple one-step chemical vapor deposition (CVD) method. Solid core-mesoporous shell silica spheres with an average diameter of ~400 nm are used as supports not only for the synthesis of the FeCo/GC nanocrystals but also for catalysts after the synthesis of the FeCo/GC@MSS. The FeCo/GC nanocrystals in the mesoporous silica spheres exhibit superparamagnetism with ultrahigh saturation magnetization up to 215 e.m.u./metal g at room temperature. The FeCo/GC@MSS is chemically stable against acid etching and oxidation, which enable the FeCo/GC@MSS to be used as a support for an acid catalyst, phosphomolybdic acid (PMA). We have shown that PMA-loaded FeCo/GC@MSS works as an excellent recyclable reagent system that catalyzes propargylation of 1,3-diphenyl-2-propyn-1-ol with phenol.

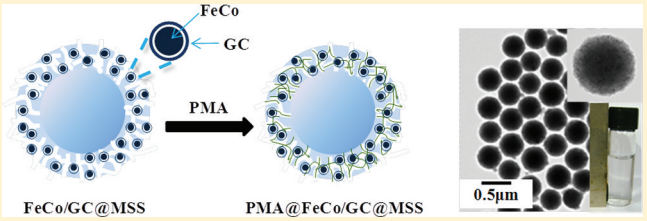

KEYWORDS: *mesoporous silica spheres, magnetic nanoparticles, FeCo, graphitic shell, supported catalysts*

INTRODUCTION

Composites with nanoparticles have been actively investigated for a wide range of applications in magnetic, catalytic, environmental, and biomedical fields.[1−15] In particular, mesoporous silica spheres (MSS) containing magnetic nanoparticles are of great interest for technological applications such as magnetic resonance imaging (MRI) contrast agents,[16−18] recyclable supporting materials,[19−21] magnetic carriers for drug-delivery,[17,22−25] and bioseparation[26] owing to their large pore size, high surface area, good chemical stability, excellent magnetic attraction to external fields, and nontoxic nature.[10] Many types of MSS with magnetic nanoparticles have been synthesized by encapsulating magnetic nanoparticles with mesoporous silica shells,[4,25] assembling magnetic nanoparticles with MSS through covalent bonding[21,22] electrostatic interaction,[17,23,24] and embedding magnetic nanoparticles into MSS.[11,12]

The magnetic nanoparticles in MSS have been mostly Fe-containing metal oxides. However, due to their inherent instability, Fe-containing metal oxides are not desirable in some cases if the nanoparticle-bearing MSS is used as a catalyst support.[25] They might affect catalytic reactions by providing an oxygen source and tend to be dissolved during catalytic reactions, eventually losing their initial magnetic attraction to external fields.[27] Therefore, it remains an important challenge to improve the stability of magnetic nanoparticles in MSS and eventually the recyclability of the MSS containing valuable catalysts.

Among all known magnetic materials, FeCo has superior magnetic properties of the highest saturation magnetization and a high superparamagnetic limit above 20 nm, but it has yet to be explored due to its easy oxidation and potential toxicity.[28−30] Recent progress on the synthesis of FeCo/graphitic carbon shell (FeCo/GC) nanocrystals by a CVD method has provided a way to solve these problems.[31] A single-layered graphitic carbon on the FeCo nanocrystal endowed it with superior stability against chemical attacks in gas and liquid phases. Recently, a highly integrated FeCo/GC nanocrystal system for combined drug delivery, imaging, and photothermal theraphy has been developed.[32]

We herein present a simple one-step CVD method to synthesize highly stable and magnetically recyclable MSS embedded with FeCo-graphitic carbon shell nanocrystals (FeCo/GC@MSS). The schematic strategy for the preparation of FeCo/GC@MSS and phosphomolybdic acid (PMA) loading is illustrated in Scheme 1. The FeCo/GC nanocrystal with a

Received: August 18, 2011
Revised: November 11, 2011
Published: November 15, 2011

Scheme 1. Schematic Diagram for the Preparation of a PMA@FeCo/GC@MSS

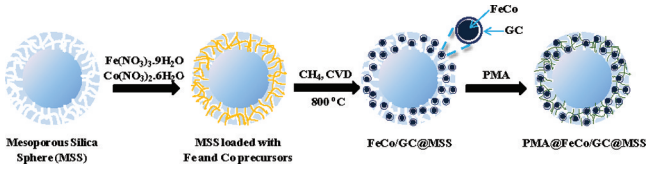

single carbon shell in the MSS exhibits superparamagnetism with ultrahigh saturation magnetization up to 215 e.m.u./metal g at room temperature. The FeCo/GC nanocrystals are chemically stable against acid etching and oxidation,[31] enabling the FeCo/GC@MSS to be used as a support for an acid catalyst, PMA. We have shown that PMA-loaded FeCo/GC@MSS works as an excellent recyclable reagent system that catalyzes propargylation of 1,3-diphenyl-2-propyn-1-ol with phenol.

RESULTS AND DISCUSSION

The synthesis of FeCo/GC@MSS is based on the previous report on the synthesis of FeCo/GC nanocrystals in fumed silica as a support.[31] Instead of the fumed silica, we used MSS as a support not only for the synthesis of FeCo/GC nanocrystals but also for the loading of PMA after the synthesis of FeCo/GC@MSS. The MSS with a solid silica core-mesoporous silica shell structure was prepared through a modified Stöber process.[33] Metal precursors, $Fe(NO_3)_3{\cdot}9H_2O$ and $Co(NO_3)_2{\cdot}6H_2O$, at a 58:42 molar ratio were loaded into the MSS by impregnation in a methanol solution and evaporation of methanol. The metal-loaded MSS was heated to 800 °C under H_2 and then subjected to methane CVD for carbon deposition on the FeCo nanocrystals formed in the MSS. Once cooled to room temperature, any metal impurities in the MSS were removed by washing with a 10% HCl solution; the resulting FeCo/GC@MSS was obtained as a light gray powder.

Figure 1a shows the transmission electron microscopy (TEM) image of the FeCo/GC@MSS. When 0.9 mmol of metals was loaded on 1.0 g of MSS, FeCo/GC nanocrystals with an average diameter of 5.6 ± 1.0 nm were formed in MSS. The mean and standard deviation of crystal sizes were measured by TEM for ~500 FeCo/GC nanocrystals obtained after treatment of the FeCo/GC@MSS with HF to dissolve the silica support (see the Supporting Information for TEM images (Figure S1)). The TEM image of a FeCo/GC@MSS in the inset of Figure 1a clearly shows the ~5.6 nm FeCo/GC nanocrystals embedded in the MSS. We identified the body-centered-cubic (bcc) crystal structure of a FeCo core for the FeCo/GC nanocrystals by electron diffraction (Figure 1b) and powder X-ray diffraction (XRD, Figure 1d). High-resolution TEM (Figure 1c) clearly shows the lattice fringes of the bcc-FeCo core (d spacing = 2.02 Å for a (110) reflection). One-layer graphitic shells overcoating the core are observed from the high-resolution TEM image of the FeCo/GC nanocrystals (see the Supporting Information (Figure S1)). The crystallite size determined for the (110) reflection of the XRD data (Figure 1d) by using the Debye–Scherrer equation[34] is 5.3 nm, which is in good agreement with the mean diameter determined from the TEM images, indicating the single-crystalline and spherical nature of individual FeCo nanocrystals.

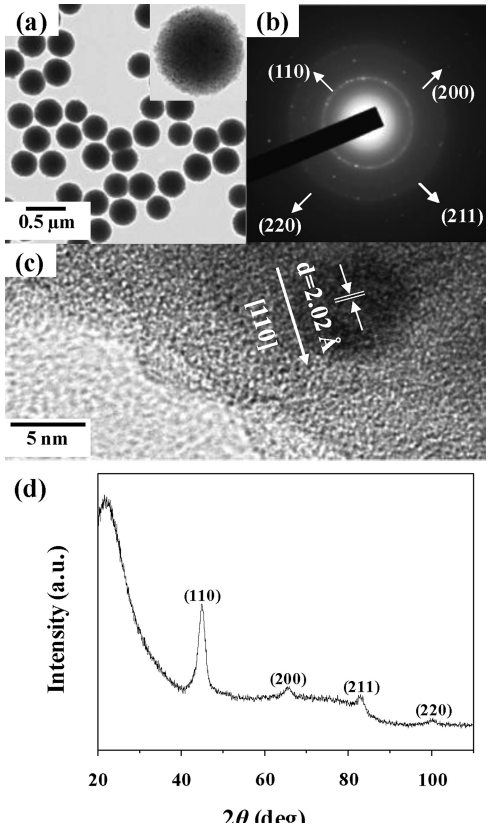

Figure 1. Structural characterization of FeCo/GC(5.6 nm)@MSS: (a) TEM image (Inset is a high magnification image.), (b) SAED pattern, (c) HRTEM image, and (d) X-ray diffraction pattern.

The average size of the FeCo/GC nanocrystals in the MSS was tunable by changing the metal loading on the MSS. When 1.8 and 0.45 mmol of metals were loaded on 1.0 g of MSS, FeCo/GC nanocrystals with average diameters of 6.7 ± 1.0 nm and 4.6 ± 1.1 nm were formed, respectively (see the Supporting Information (Figure S1)). Figure 2a and b shows the TEM images of FeCo/GC(6.7 nm)@MSS and FeCo/GC(4.6 nm)@MSS. The bcc FeCo crystal structure was retained for the ~6.7 nm and ~4.6 nm FeCo/GC nanocrystals as indicated by the XRD data in Figure 2c.

Energy dispersive X-ray (EDX) analysis for the emission of the samples shows Fe/Co ratios of 52:48, 50:50, and 47:53 for the ~6.7 nm, ~5.6 nm, and ~4.6 nm FeCo/GC nanocrystals (see the Supporting Information (Figure S3)). The Fe/Co ratios also very well match with the data obtained from the calcination/HCl/ultraviolet–visible method reported previously.[31] We employed a 58:42 molar ratio of the Fe and Co metal precursors to synthesize FeCo/GC nanocrystals with about 1:1 ratios of Fe and Co. It was based on the previous report that FeCo nanocrystals with Co richness were prepared when the same amounts of Fe and Co precursors were employed.[31] As we expected, FeCo/GC nanocrystals with roughly 1:1 Fe/Co ratios were obtained from the Fe and Co metal precursors with Fe richness. Moreover, the Fe/Co ratios of FeCo/GC nanocrystals were retained within 5% variation during the 4-fold increase in the metal loading on MSS, which is remarkable considering a previous study reported an Fe/Co ratio change from 40:60 to Co-dominant 12:88, giving a mixture of FeCo and face-centered-cubic (fcc) Co.[31] The difference between the Fe/Co ratios of the precursors and of

dx.doi.org/10.1021/cm202451n | Chem. Mater. 2011, 23, 5398–5403

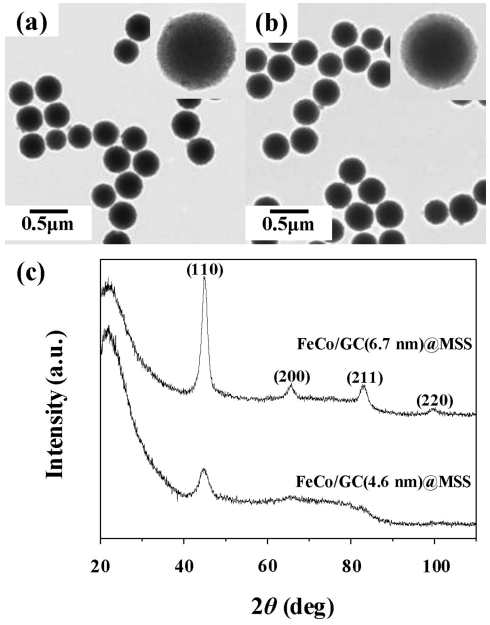

Figure 2. Structural characterization of FeCo/GC(6.7 nm)@MSS and FeCo/GC(4.6 nm)@MSS: TEM images of (a) FeCo/GC(6.7 nm)@MSS and (b) FeCo/GC(4.6 nm)@MSS (Insets are high magnification images.) and (c) X-ray diffraction patterns.

the products is due to the different decomposition characteristics of the former, which eventually offer different molar concentrations of the growth species. The small variation in the Fe/Co ratios of the products prepared in MSS can be attributed to the confined decomposition condition of the metal precursors. Though they are not generated at the same time, the growth species prepared from the decomposition of the metal precursors may have roughly the same Fe and Co molar concentrations at the crystal growth time since they are not able to easily move away from the decomposition place in MSS.

Magnetization measurements were performed with a superconducting quantum interference device-vibrating sample magnetometer (SQUID-VSM). To determine the total metal amount for the magnetization measurements, we used the same calcination/HCl/ultraviolet−visible method above-mentioned. The saturation magnetization (M_s) values were 215 e.m.u./metal g, 211 e.m.u./metal g, and 205 e.m.u./metal g for the ~6.7 nm, ~5.6 nm, and ~4.6 nm FeCo/GC nanocrystals, respectively (see the Supporting Information (Figure S4a)). It is noteworthy that the ~4.6 nm FeCo/GC sample, the smallest among the samples, also had very high M_s close to that of a bulk FeCo (235 e.m.u./g). This is due to the single crystalline bcc structure of the FeCo/GC nanocrystals without containing any fcc Co phase. As seen in Figure S4b (Supporting Information), the divergence between the zero-field-cooled (ZFC) and field-cooled (FC) data as well as the ferromagnetic-like behavior without hysteresis at 300 K is indicative of the characteristics of a superparamagnetic system. The blocking temperatures (T_B) at 100 Oe, where the ZFC curve exhibits a maximum, were 125 K, 75 K, and 42 K for the ~6.7 nm, ~5.6 nm, and ~4.6 nm FeCo/GC samples, respectively. This result is consistent with the linear relationship between the crystal volume V and T_B as predicted from the equation $KV = 25k_BT_B$,[35,36] where K is the anisotropy constant and k_B is the Boltzmann's constant. It should be noted that T_B shifts to a lower value with a larger applied field.

The surface area and the porosity of the MSS embedded with ~5.6 nm FeCo/GC nanocrystals (FeCo/GC(5.6 nm)@MSS) were investigated by using nitrogen adsorption−desorption isotherms (see the Supporting Information). The BET (Brunauer−Emmett−Teller) surface area, total pore volume, and calculated average pore diameter were found to be 315.8 m^2/g, 0.239 cm^3/g, and 2.9 nm, respectively, which are a little smaller than those of MSS (343.8 m^2/g, 0.312 cm^3/g, and 3.1 nm) due to the embedment of the ~5.6 nm FeCo/GC nanocrystals into the MSS. Nevertheless, they show the same type IV isotherm which is typical for mesoporous silica,[37] indicating that their pores might have a large enough inner space to undergo some catalytic reactions.

To investigate the functionality of the FeCo/GC@MSS as a recyclable support for acid catalysts, we loaded PMA on the FeCo/GC(5.6 nm)@MSS. PMA supported on silica gel has been recently reported as an efficient system for selective deprotection of tert-butyldimethylsilyl ether[38] and the synthesis of homoallyl alcohols and amines.[39] In this study, we have used the PMA-loaded FeCo/GC(5.6 nm)@MSS (PMA@FeCo/GC(5.6 nm)@MSS) to catalyze the propargylation of 1,3-diphenyl-2-propyn-1-ol with phenol. Recently, there have been intensive studies over propargylic substitution reactions, in which activated and inactivated propargyl alcohols, propargyl acetates, and/or propargyl esters are reacted with alcohols, thiols, amines, and such that have C-nucleophiles and heteroatom-centered nucleophiles.[40,41] However, the recovery and reuse of the catalysts still remain a challenge.

We prepared PMA@FeCo/GC(5.6 nm)@MSS (10 wt % of PMA in SiO_2) as a light greenish powder by adding FeCo/GC(5.6 nm)@MSS to a methanol solution of PMA, sonicating for 5 min and stirring for 6 h at room temperature, and evaporating the methanol. Figure 3a shows the TEM images of the PMA@FeCo/GC(5.6 nm)@MSS. The ~5.6 nm FeCo/GC nanocrystals embedded in a mesoporous silica sphere are still clearly observed (inset of Figure 3a). Furthermore, the XRD data of the PMA@FeCo/GC(5.6 nm)@MSS (Figure 3e red) are almost the same as that of the FeCo/GC(5.6 nm)@MSS without being broadened due to the chemical etching of the FeCo nanocrystals, clearly demonstrating the chemical stability of the FeCo/GC(5.6 nm)@MSS. We prepared FeCo nanocrystals without being encapsulated with carbon shells in the MSS (FeCo@MSS) to compare the chemical stability of FeCo/GC@MSS and FeCo@MSS. The TEM images of the FeCo(5.6 nm)@MSS (Figure 3b) also show the ~5.6 nm FeCo nanocrystals embedded in the MSS, and the XRD data collected right after the synthesis of the sample (Figure 3e blue) still indicate the bcc FeCo crystal structure. However, we cannot observe any FeCo nanocrystals from the TEM images (Figure 3c) of the FeCo@MSS sample after the aforementioned PMA-loading procedure owing to the FeCo etching by PMA. The XRD data of the sample (Figure 3e black) also do not display any reflections of the crystal planes. As shown in the inset of Figure 3c, the color of the sample in a water suspension is brown, which is different from the dark grayish brown color of the PMA@FeCo/GC(5.6 nm)@MSS suspension in the inset of Figure 3a. When these samples were placed next to a cubic NbFeB magnet, only the PMA@FeCo/GC(5.6 nm)@MSS was attracted very quickly, whereas the PMA-treated FeCo(5.6 nm)@MSS was not attracted by the magnet due to the loss of the FeCo nanocrystals (Figure 3d). This clearly demonstrates that only the FeCo/GC@MSS is stable in the presence of acids and thus able to support acid catalysts since metal or metal oxide

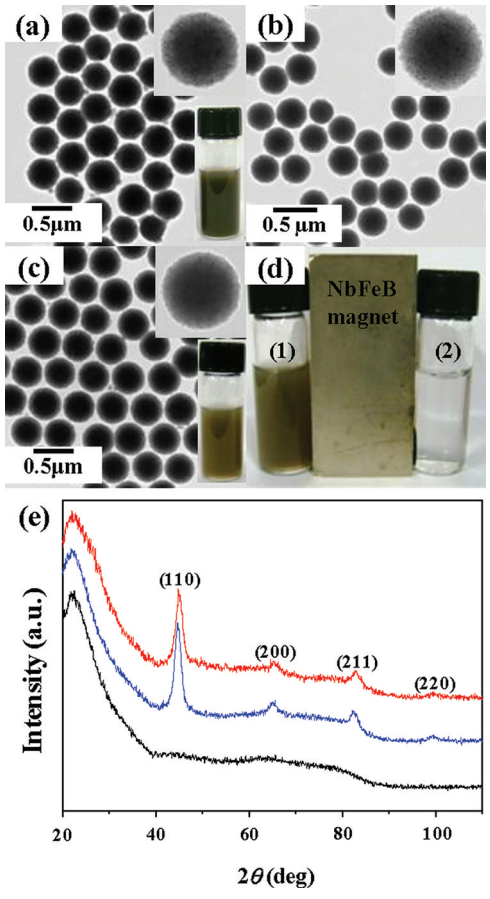

Figure 3. TEM images of (a) PMA@FeCo/GC(5.6 nm)@MSS, (b) FeCo(5.6 nm)@MSS, and (c) FeCo(5.6 nm)@MSS after the PMA-loading procedure (Insets are higher magnification images (a-c) and photographs of H_2O solutions of PMA@FeCo/GC(5.6 nm)@MSS (a) and FeCo(5.6 nm)@MSS after the PMA-loading procedure (c).) (d) A photograph of (1) PMA-treated FeCo(5.6 nm)@MSS and (2) PMA@FeCo/GC(5.6 nm)@MSS in water after 5 min in the presence of a cubic NbFeB magnet. (e) XRD patterns of PMA@FeCo/GC(5.6 nm)@MSS (red), FeCo(5.6 nm)@MSS (blue), and PMA-treated FeCo(5.6 nm)@MSS (black).

magnetic nanoparticles without being encapsulated with graphitic carbon shells such as FeCo, iron oxides, and ferrites are not very stable against chemical attacks in liquid phase.

We additionally investigated long-term chemical stability of the FeCo/GC@MSS in air and water. After the synthesis of the FeCo(5.6 nm)/GC@MSS, we stored the sample over a monitoring period of two months in air and water, respectively, and added a 35% HCl solution to the samples. The two FeCo/GC(5.6 nm)@MSS samples still exhibited excellent stability against HCl etching. However, as-prepared FeCo(5.6 nm)@MSS, in which the FeCo nanocrystals were not encapsulated with carbon shells, turned the color of the solution to green right after the addition of a 35% HCl solution owing to the Fe and Co etching (see the Supporting Information (Figure S5)). This means that FeCo/GC@MSS is still stable against oxidation for a long time in air and water due to the robustness of the single-layered graphitic shell.

We conducted preliminary experiments on the propargylation reactions of 1,3-diphenyl-2-propyn-1-ol with phenol to yield the expected 4-(1,3-diphenyl-2-propynyl)phenol with the PMA@FeCo/GC(5.6 nm)@MSS catalyst and tested the recyclability of the catalyst (Scheme 2 and Table 1). The

Scheme 2. Reaction Scheme for Propargylation of 1,3-Diphenyl-2-propyn-1-ol with Phenol by the PMA@FeCo/GC@MSS Catalyst

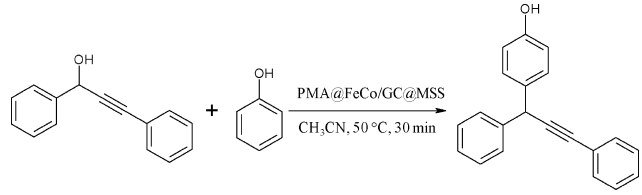

Table 1. Propargylation of 1,3-Diphenyl-2-propyn-1-ol with Phenol Using Efficient Recyclable PMA@FeCo/GC(5.6 nm)@MSS[a]

entry	catalyst (PMA mol %)	time (min)	temp (°C)	conv. (%)[b]	TOF (h^{-1})
1	0.1 mol % PMA@FeCo/GC@MSS	30	25	93	1860
2	0.03 mol % PMA@FeCo/GC@MSS	30	50	79	5267
3	0.05 mol % PMA@FeCo/GC@MSS	30	50	100	4000
4	0.05 mol % PMA@FeCo/GC@MSS	5	50	81	19440
5	0.05 mol % PMA	30	50	95	3800
6	FeCo/GC@MSS	30	50	0	
7	MSS	30	50	0	
8	recovered from # 3 (second use)	30	50	100	4000
9	recovered from # 8 (third use)	30	50	100	4000
10	recovered from # 9 (fourth use)	30	50	100	4000
11	recovered from # 10 (fifth use)	30	50	100	4000

[a]Reaction conditions: 1,3-diphenyl-2-propyn-1-ol (0.19 mL, 1.0 mmol), phenol (0.113 g, 1.2 mmol), acetonitrile (5.0 mL). [b]Determined by ^{1}H NMR spectroscopy. Yields are based on the amount of propargylic alcohol.

amount of catalyst, reaction temperature, and reaction time were adjusted to maximize reaction activity. In general, it was found that increasing the amount of catalyst, reaction temperature, and time were effective means of increasing conversion (Table 1, entries 1–4). Under common conditions at 323 K, the conversion approaches 100% during the reaction time of 30 min where 0.05 mol % PMA is present (Table 1, entry 3). In addition, no reaction occurred in the absence of PMA even though those optimized reaction conditions remained (Table 1, entries 6 and 7). In actuality, the PMA@FeCo/GC(5.6 nm)@MSS catalysts were separated from the clean solution after the reaction by a magnet, and the separated catalysts were used further for the propargylation reactions of 1,3-diphenyl-2-propyn-1-ol with phenol at least five times without loss of catalytic activity (Table 1, entries 3, 8–11), demonstrating the recyclability of the PMA@FeCo/GC(5.6 nm)@MSS catalysts. The TEM image of the PMA@FeCo/GC(5.6 nm)@MSS catalyst after the five consecutive catalytic cycles also demonstrates that the catalyst still remains the same (see the Supporting Information (Figure S6)).

■ CONCLUSIONS

In conclusion, we synthesized MSS embedded with FeCo/GC nanocrystals by a simple one-step CVD process. The size (4.6–

dx.doi.org/10.1021/cm202451n | Chem. Mater. 2011, 23, 5398–5403

6.7 nm) and the amount of FeCo/GC nanocrystals in MSS can be readily tuned by varying the amount of metal precursors loaded in MSS. We demonstrated the preparation of the superparamagnetic FeCo/GC(5.6 nm)@MSS with high saturation magnetization and superior chemical stability against acid etching and oxidation. PMA-loaded FeCo/GC(5.6 nm)@MSS was used as a recyclable catalyst for propargylation reactions. Our composite system may offer an opportunity for economically and environmentally benign highly stable catalyst support for various catalytic reactions including organic catalytic reactions and photocatalytic reactions in solutions.

EXPERIMENTAL SECTION

General Methods. $Fe(NO_3)_3{\cdot}9H_2O$ (99.99%, Aldrich), $Co(NO_3)_2{\cdot}6H_2O$ (99.999%, Aldrich), $H_3PMo_{12}O_{40}{\cdot}24H_2O$ (phosphomolybdic acid (PMA) hydrate, 99.99%, Aldrich), TEOS (tetraethoxysilane, 98%, Aldrich), and C18TMS (n-octadecyltrimethoxysilane, 85%, TCI) were used without further purification. All other reagents purchased from commercial sources were used as obtained without further purification.

Preparation of PMA@FeCo/GC@MSS. (a) Mesoporous Silica Spheres (MSS). Mesoporous silica spheres composed of mesoporous shell and solid core with average diameter of about 400 nm were prepared through a modified Stöber process.[32] In a 250 mL round-bottom flask, 75 mL of ethanol, 10 mL of deionized water, and 3 mL of ammonia were mixed, and the mixture was stirred for 10 min. To the solution was added 6 mL of TEOS, and the solution was vigorously stirred. After stirring for 2 h, a mixture of 5 mL of TEOS and 2 mL of C18TMS was added under vigorous stirring for 2 h. The resulting solid core/mesoporous shell silica spheres were collected by centrifugation and then dried in air to yield a white powder. To remove all organic residues incorporated in the silica, we sintered the powder in air at 823 K for 6 h. **(b) FeCo/GC@MSS and FeCo/GC Nanocrystals.** For 4.6 nm FeCo/GC@MSS, we impregnated 1.00 g of MSS with 0.11 g (0.26 mmol) of $Fe(NO_3)_3{\cdot}9H_2O$ and 0.06 g (0.19 mmol) of $Co(NO_3)_2{\cdot}6H_2O$ in 50 mL of methanol and sonicated it for 1 h. For FeCo/GC(5.6 nm)@MSS and 6.7 nm FeCo/GC@MSS, we used the metal loading 2 times and 4 times, respectively. After removal of methanol and drying at 80 °C, we ground the powder and typically used 0.50 g for methane CVD in a tube furnace. We heated the sample in a H_2 flow to reach 800 °C and then subjected it to a methane flow of 500 cm^3 min^{-1} for 5 min. On cooling, we washed the samples with ethanol and collected them by centrifugation. To obtain the FeCo/GC nanocrystals, we etched the samples with 15% HF in H_2O (75%) and ethanol (10%) to dissolve the silica. We collected the FeCo/GC nanocrystals by centrifugation and thoroughly washed them. **(c) PMA@FeCo/GC(5.6 nm)@MSS.** 0.82 g of FeCo/GC(5.6 nm)@MSS nanoparticles was added slowly to a solution of $H_3PMo_{12}O_{40}{\cdot}24H_2O$ (0.09 g, 0.05 mmol) in 10 mL of methanol. The mixture was stirred at room temperature for 6 h. Evaporation of methanol under reduced pressure gave a greenish black powder, which contained 10 wt % of PMA in SiO_2.

Preparation of FeCo(5.6 nm)@MSS. The procedure for the synthesis of FeCo(5.6 nm)@MSS is similar to that of FeCo/GC(5.6 nm)@MSS. Instead of a methane flow at 800 °C for 5 min, H_2 was flowed.

Characterization. We characterized nanocrystals by XRD (Rigaku Miniflex II (4.5 KW) diffractometer using Cu−Kα radiation at 30 kV and 15 mA), TEM (JEOL JEM-2100F operated at 200 KV) with selected area electron diffraction (SAED) patterns, and energy dispersive analyses of X-ray emission (EDX). Samples for TEM investigations were prepared by dropping the diluted sample in ethanol on a 300 mesh carbon support copper grid (Ted Pella, Inc.). The magnetic measurements were performed on a SQUID magnetometer (Quantum Design MPMS SQUID-VSM). DC susceptibility and hysteresis measurements were recorded for powdered samples in a gelatin capsule. The temperature was varied between 2 and 300 K according to a zero field cooling/field cooling (ZFC/FC) procedure at 100 Oe, and the hysteretic loops were obtained in a magnetic field varying from +7 to −7 T.

Nitrogen Sorption Measurements. Adsorption and desorption measurements were performed using a BELSORP-max instrument with nitrogen. The BET surface areas were calculated from p/p_0 = 0.05−0.30 in the adsorption curve using a BET equation. Prior to each sorption measurement, the sample was outgassed at 300 °C for 24 h under vacuum to remove all the impurities completely.

Propargylation Catalyzed by the PMA@FeCo/GC(5.6 nm)@MSS Catalyst. In a 10 mL Schlenk pressure tube were added the PMA@FeCo/GC(5.6 nm)@MSS catalyst (0.05 mol %), 1,3-diphenyl-2-propyn-1-ol (0.19 mL, 1.0 mmol), phenol (0.113 g, 1.2 mmol), and acetonitrile (5.0 mL). The mixture was stirred at 323 K for 30 min. After the reaction, the catalyst was separated from the clean solution by a magnet. The reaction products were analyzed by using a ^1H NMR Varian Mercury Plus spectrometer (300 MHz). Chemical shift values were recorded as parts per million relative to tetramethylsilane as an internal standard unless otherwise indicated, and coupling constants were in Hertz.

ASSOCIATED CONTENT

Supporting Information

TEM images, XRD patterns, SQUID data, EDX data. This material is available free of charge via the Internet at http://pubs.acs.org.

AUTHOR INFORMATION

Corresponding Author

*E-mail: wsseo@sogang.ac.kr (W.S.S), chemistry@pusan.ac.kr (K.H.P).

ACKNOWLEDGMENTS

This research was supported by the Basic Science Research Program through the National Research Foundation of Korea (NRF) funded by the Ministry of Education, Science and Technology (2011-0002773). K.H.P. thanks the support of the Basic Science Research Program through the NRF of Korea funded by the Ministry of Education, Science and Technology (2010-0002834). M.H.J. thanks the support of the IT R&D program of MKE/KEIT Grant No. 2009-F-004-01. N.H.H. thanks the NRL program (2010-0018937) funded by the Ministry of Education, Science, and Technology through the NRF of Korea.

REFERENCES

(1) Zhao, Y.; Jiang, L. *Adv. Mater.* **2009**, *21*, 3621.
(2) Lou, X. W.; Archer, L. A.; Yang, Z. *Adv. Mater.* **2008**, *20*, 3987.
(3) Giri, S.; Trewyn, B. G.; Stellmaker, M. P.; Lin, V. S.-Y. *Angew. Chem., Int. Ed.* **2005**, *44*, 5038.
(4) Levy, L.; Sahoo, Y.; Kim, K. S.; Bergey, E. J.; Prasad, P. N. *Chem. Mater.* **2002**, *14*, 3715.
(5) Liang, C.; Li, Z.; Dai, S. *Angew. Chem., Int. Ed.* **2008**, *47*, 3696.
(6) Xu, Z.; Hou, Y.; Sun, S. *J. Am. Chem. Soc.* **2007**, *129*, 8698.
(7) Lee, J.; Kim, J.; Hyeon, T. *Adv. Mater.* **2006**, *18*, 2073.
(8) Yavuz, C. T.; Mayo, J. T.; Yu, W. W.; Prakash, A.; Falkner, J. C.; Yean, S.; Cong, L.; Shipley, H. J.; Kan, A.; Tomson, M.; Natelson, D.; Colvin, V. L. *Science* **2006**, *314*, 964.
(9) Ge, J.; Hu, Y.; Biasini, M.; Beyermann, W. P.; Yin, Y. *Angew. Chem., Int. Ed.* **2007**, *46*, 4342.
(10) Lu, Y.; Yin, Y.; Mayers, B. T.; Xia, Y. *Nano Lett.* **2002**, *2*, 183.
(11) Lee, K. R.; Kim, S.; Kang, D. H.; Lee, J. I.; Lee, Y. J.; Kim, W. S.; Cho, D. H.; Lim, H. B.; Kim, J.; Hur, N. H. *Chem. Mater.* **2008**, *20*, 6738.
(12) Lee, B. S.; Yi, M.; Chu, S. Y.; Lee, J. Y.; Kwon, H. R.; Lee, K. R.; Kang, D.; Kim, W. S.; Lim, H. B.; Lee, J.; Youn, H. J.; Chi, D. Y.; Hur, N. H. *Chem. Commun.* **2010**, *46*, 3935.

(13) Chaubey, G. S.; Barcena, C.; Poudyal, N.; Rong, C.; Gao, J.; Sun, S.; Liu, J. P. *J. Am. Chem. Soc.* **2007**, *129*, 7214.
(14) Xia, Y.; Yang, P.; Sun, Y.; Wu, Y.; Mayers, B.; Gates, B.; Yin, Y.; Kim, F.; Yan, H. *Adv. Mater.* **2003**, *15*, 353.
(15) Jeong, B. U.; Teng, X.; Wang, Y.; Yang, H.; Xia, Y. *Adv. Mater.* **2007**, *19*, 33.
(16) Choi, J.; Lee, J . H.; Shin, T. H.; Song, H. T.; Kim, E. Y.; Cheon, J. *J. Am. Chem. Soc.* **2010**, *132*, 11015.
(17) Kim, J.; Kim, H. S.; Lee, N.; Kim, T.; Kim, H.; Yu, T.; Song, I. C.; Moon, W. K.; Hyeon, T. *Angew. Chem., Int. Ed.* **2008**, *47*, 8438.
(18) Jun, Y.; Lee, J. H.; Cheon, J. *Angew. Chem., Int. Ed.* **2008**, *47*, 5122.
(19) Ge, J; Zhang, Q.; Zhang, T.; Yin, Y. *Angew. Chem., Int. Ed.* **2008**, *47*, 8924.
(20) Ge, J.; Huynh, T.; Hu, Y.; Yin, Y. *Nano Lett.* **2008**, *8*, 931.
(21) Shokouhimehr, M.; Piao, Y.; Kim, J.; Jang, Y.; Hyeon, T. *Angew. Chem., Int. Ed.* **2007**, *46*, 7039.
(22) Zhao, W.; Gu, J.; Zhang, L.; Chen, H.; Shi, J. *J. Am. Chem. Soc.* **2005**, *127*, 8916.
(23) Lin, Y. S.; Wu, S. H.; Hung, Y.; Chou, Y. H.; Chang, C.; Lin, M. L.; Tsai, C. P.; Mou, C. Y. *Chem. Mater.* **2006**, *18*, 5170.
(24) Deng, Y.; Qi, D.; Deng, C.; Zhang, X.; Zhao, D. *J. Am. Chem. Soc.* **2008**, *130*, 28.
(25) Kim, J.; Lee, J. E.; Lee, J.; Yu, J. H.; Kim, B. C.; An, K.; Hwang, Y.; Shin, C. H.; Park, J. G.; Kim, J.; Hyeon, T. *J. Am. Chem. Soc.* **2006**, *128*, 688.
(26) Xu, X.; Deng, C.; Gao, M.; Yu, W.; Yang, P.; Zhang, X. *Adv. Mater.* **2006**, *18*, 3289.
(27) Ye, M.; Zhang, Q.; Hu, Y.; Ge, J.; Lu, Z.; He, L.; Chen, Z.; Yin, Y. *Chem.—Eur. J.* **2010**, *16*, 6243.
(28) Hütten, A.; Sudfeld, D.; Ennen, I.; Reiss, G.; Hachmann, W.; Heinzmann, U.; Wojczykowski, K.; Jutzi, P.; Saikaly, W.; Thomas, G. *J. Biotechnol.* **2004**, *112*, 47.
(29) Mcguire, T. R. *Appl. Phys.* **1969**, *40*, 1371.
(30) Reiss, G.; Hütten, A. *Nat. Mater.* **2005**, *4*, 725.
(31) Seo, W. S.; Lee, J. H.; Sun, X. M.; Suzuki, Y.; Mann, D.; Liu, Z.; Terashima, M.; Yang, P. C.; Mcconnell, M. V.; Nishimura, D. G.; Dai, H. *Nat. Mater.* **2006**, *5*, 971.
(32) Sherlock, S. P.; Tabakman, S. M.; Xie, L.; Dai, H. *ACS Nano* **2010**, *5*, 1505.
(33) Büchel, G.; Unger, K .K.; Matsumoto, A.; Tsutsumi, K. *Adv. Mater.* **1998**, *10*, 1036.
(34) Cullity, B. D. *Elements of X-ray Diffraction*; Addison-Wesley: Reading, MA, 1978.
(35) Bean, C. P.; Livingston, J. D. *J. Appl. Phys.* **1959**, *30*, 120S.
(36) Seo, W. S.; Jo, H. H.; Lee, K.; Kim, B.; Oh., S. J.; Park, J. T. *Angew. Chem., Int. Ed.* **2004**, *43*, 1115.
(37) Brunauer, S.; Deming, L S.; Deming, W. E.; Teller, E. *J. Am. Chem. Soc.* **1940**, *62*, 1723.
(38) Kishore Kumar, G. D.; Baskaran, S. *J. Org. Chem.* **2005**, *70*, 4520.
(39) Das, B.; Kumar, R. A.; Thirupathi, P.; Suneel, K.; Sunitha, P. *Can. J. Chem.* **2008**, *86*, 709.
(40) Yadav, J. S.; Subba Reddy, B. V.; Raghavendra Rao, K. V.; Narender, R. *Tetrahedron Lett.* **2009**, *50*, 3963.
(41) Srihari, P.; Bhunia, D. C.; Sreedhar, P.; Mandal, S. S.; Sunder Reddy, J. S.; Yadav, J. S. *Tetrahedron Lett.* **2007**, *48*, 8120.